Green Chemistry

Accepted Manuscript

ROYAL SOCIETY OF CHEMISTRY

www.rsc.org/greenchem

Green Chemistry

PAPER

Multifunctional natural agarose as an alternative material for high-performance rechargeable lithium-ion batteries†

Received 00th January 20xx,
Accepted 00th January 20xx

DOI: 10.1039/x0xx00000x

www.rsc.org/

Gaeun Hwang[a], Ju-Myung Kim[a], Dongki Hong[a], Choon-Ki Kim[a], Nam-Soon Choi[a], Sang-Young Lee*[a] and Soojin Park*[a]

An agarose, one of natural polysaccharides that are generally extracted from seaweeds, has recently attracted great attention as an environmentally-benign building element for a wide variety of applications. Notably, its disaccharide repeating units bearing ether/hydroxyl groups bring unprecedented performance benefits far beyond those accessible with traditional synthetic polymers. Herein, intrigued by such unusual chemical features of the agarose, we explore its potential applicability as an alternative electrode binder and also a carbon source for high-performance rechargeable lithium-ion batteries. The agarose binder enables silicon (Si) active materials to be tightly adhered to copper foil current collectors, thereby providing significant improvement in electrochemical performance of the resultant Si anode (specific capacity = 2000 mAh g^{-1} and capacity retention after 200 cycles = 71%). In addition, the agarose can be exploited as a cathode binder. The $LiMn_2O_4$ cathode containing the agarose binder shows the excellent cell performance (initial coulombic efficiency ~ 96.2% and capacity retention after 400 cycles ~100 %). Through the selective carbonization of Si-dispersed agarose, the Si/C (hard carbon) composite active materials are successfully synthesized. Eventually, the Si/C composite anode and the $LiMn_2O_4$ cathode mentioned above are assembled to produce a full cell featuring the use of agarose as an alternative green material. Benefiting from the exceptional multifuctionality of agarose, the full cell presents the stable cycling performance (capacity retention after 50 cycles >87%).

Introduction

Lithium-ion batteries (LIBs) have well-balanced performance attributes such as light weight, high working voltage, high energy density, long cycle life and no memory effect, which thus allow their predominant position as a competent power source for a vast variety of portable electronic devices.[1-3] Spurred by the remarkable success in the mobile applications, LIBs are currently eager to extend their applications to newly emerging energy fields such as electric vehicles and grid-scale energy storage systems. To facilitate this application extension and also consolidate their strong position as a portable power source, the LIBs need to relentlessly pursue higher energy/power density. Unfortunately, conventional battery materials are not sufficient to address the aforementioned energy/power challenges, thus pushing us to search for new alternative materials with reliable electrochemical performances.[4-6]

Silicon (Si) has attracted much attention as a promising anode material because of its high theoretical capacity (3579 mAh g^{-1}), natural abundance, and low cost.[7-10] However, a large volume change of > 300% during lithiation-delithiation processes gives rise to serious pulverization of Si powders, continuous formation of unstable solid-electrolyte-interphase (SEI) layers, and depletion of electrolyte, eventually resulting in a rapid decay in charge/discharge capacity with cycling. In addition, Si suffers from low electrical conductivity and sluggish lithium-ion diffusivity. These fatal flaws pose formidable obstacles to impede commercialization of Si anode in LIBs.[11-13]

Numerous approaches have been suggested to overcome these drawbacks, including Si composites with metal oxide, inactive metals, or carbon materials,[14-19] and Si nanostructuring (e.g., nanoparticles,[20] nanowires,[21] and nanotubes,[22] meso/macroporous structure,[23] hollow spheres,[24] and yolk-shell[25]). Among these Si-based materials reported to date, Si/carbon (Si/C) composites showed long cycle life and excellent rate performance because carbon contributes to improving electrical conductivity of Si and acts as a buffer matrix which can accommodate large volume change of Si.[14,16,17]

Along with the direct modification of Si active materials mentioned above, another attempt has been implemented to develop

[a] Department of Energy Engineering, School of Energy and Chemical Engineering, Ulsan National Institute of Science and Technology (UNIST), UNIST-gil 50, Ulsan 44919, Republic of Korea
spark@unist.ac.kr; Fax: +82-52-217-2909; Tel: +82-52-217-2515.
syleek@unist.ac.kr; Fax: +82-52-217-2909; Tel: +82-52-217-2948

† Electronic Supplementary Information (ESI) available: Rate capabilities of agarose-assisted Si electrode and manganese ion capturing of agarose binders. See DOI : XXX

advanced polymeric anode binders which can effectively anchor Si active materials to current collectors. Until now, polyvinylidene fluoride (PVdF) has been the most widely used binder for conventional LIB electrodes. However, in Si anodes suffering from serious volume expansion, the PVdF binder is known to be inadequate for suppressing the pulverization of Si electrodes.[26-28] As alternative binders to outperform the PVdF binder, carboxymethyl cellulose (CMC),[26] poly(acrylic acid) (PAA),[29] polyamide imide (PAI),[28] alginate extracted from brown algae,[30] NaOH-neutralized poly(acrylic acid),[31] PAA/CMC,[32] agarose/PAA,[33] and hyperbranched β-cyclodextrin polymer[34] were reported. In addition, new cathode binders were developed with a particular use in $LiMn_2O_4$ (LMO) cathode, including poly(acrylonitrile-methyl methacrylate),[35] PAA, polyvinyl alcohol (PVA), polyacrylonitrile (PAN), alginate,[36] and lithiated perfluorosulfonate ionomer.[37] For example, alginate binder partially resolved the problem of Mn^{2+} dissolution.[36] Lithiated perfluorosulfonate ionomer exhibited the lower interface resistance, leading to higher capacity and cycling stability under harsh conditions (high rate of 5-20 C and high temperature of 60 °C).[37]

Among the various binder materials reported to date, significant attention should be dedicated to agarose due to its unique chemical functionality. Agarose, one of natural polysaccharides that are generally extracted from seaweeds, is a linear polymer having the repeating unit of agarobiose (composed of D-galactose and 3,6-anhydro-L-galactopyranose).[38,39] In addition to the application as an anode binder, agarose was exploited as a building element for battery separators. The agarose-based electrospun nanofiber mats effectively chelated manganese ions (Mn^{2+}) that were dissolved from LMO cathodes, thus leading to significant improvement in high-temperature cycling performance.[40]

Herein, intrigued by the unique biofunctionality of natural agarose, we explore its potential applicability as an alternative electrode binder and a carbon source for high-performance rechargeable lithium-ion batteries. The agarose binder, owing to the presence of functional groups such as ether and hydroxyl groups, allows strong adhesion between Si active material and copper current collectors, thereby providing remarkable improvement in electrochemical performance of the resultant Si anode (specific capacity = 2000 mAh g^{-1} and capacity retention after 200 cycles = 71%). The Si/C composites, which are generated through carbonization of Si-dispersed agarose, significantly enhance initial coulombic efficiency and specific capacity compared to hard carbon (synthesized from pure agarose). Meanwhile, LMO cathode adopting agarose binder shows high initial coulombic efficiency of 96.2% and outstanding cycling retention of nearly 100 % after 400 cycles. More notably, the full cell consisting of the Si/C anode and the LMO cathode mentioned above presents stable cycling performance (capacity retention after 50 cycles >87%), demonstrating the advantageous effects of agarose as a multifunctional green battery material.

Results and Discussion

Synergistic coupling of nanostructured Si and agarose binder on electrochemical tests

Nanostructured Si powders were prepared via a simple chemical etching of Al-Si alloy powder according to the previously reported procedures.[41,42] Scanning electron microscopy (SEM) image shows that Al-Si particles are spherical in shape and have diameter of 1-6 μm (fig. 1a). The Al-Si powders were then immersed into 3M hydrochloric acid (HCl) solution under mild stirring at room temperature for 1 h, producing the nanostructured Si particles comprising a number of thin frameworks (thickness = 50-100 nm) with a destruction of the original spherical shape (fig. 1b and inset).

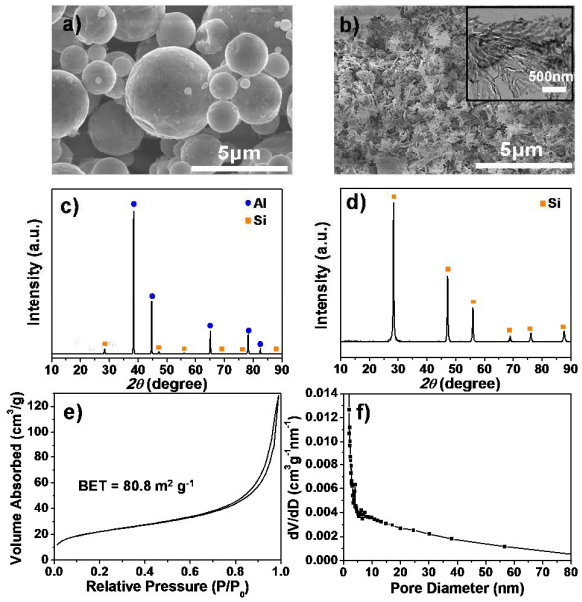

Fig. 1 SEM images of (a) pristine Al-Si powder and (b) chemically etched nanostructured Si (inset: TEM image of Si showing porous structure). XRD patterns of (c) Al-Si alloy and (d) chemically etched Si. (e) Nitrogen adsorption and desorption isotherm curve and (f) BJH plot showing the pore size distribution of nanostructured Si.

The X-ray diffraction (XRD) patterns of pristine Al-Si alloy reveal that its composition ratio is Al of ~90% and Si of ~10% (fig. 1c). After chemical etching, the characteristic peaks corresponding to pure Si were only observed, while the Al peaks completely disappeared (fig. 1d). In order to determine porosity of nanostructured Si particles, nitrogen adsorption–desorption measurements were performed (fig. 1e). The specific surface area of the Si powders, which was calculated by the Brunauer–Emmett–Teller (BET) equation, was estimated to be 80.8 m^2 g^{-1}. The pore size distribution curve, which was retrieved with the Barrett-Joyner-Halenda (BJH) model, showed that the nanostructured Si particles possess a significant portion of nanopores (fig. 1f).

The nanostructured Si powders featuring the structural uniqueness are expected to alleviate the unwanted volume change of Si during lithiation-delithiation processes, which would lead to significant improvement in cycling performance. However, the nanostructuring of Si powders is not sufficient to

fully resolve the serious volume change (>300%) of Si. Thus, a new approach should be added to overcome the limitation of the nanostructured Si powders. Here, we propose that natural agarose could be combined as an alternative binder with the nanostructured Si powders, eventually brining a synergistic coupling effect on cycling performance.

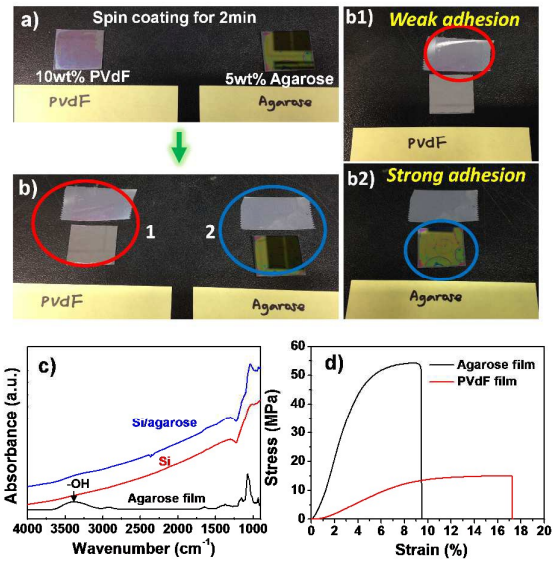

Fig. 2 (a) Photographic images of PVdF and Agarose films coated on Si wafer. (b) Peel-off tests of PVdF and agarose films using 3M scotch tape (b1: PVdF coated Si wafer; b2: agarose coated Si wafer). (c) FT-IR spectra of agarose film, Si powder, and electrode consisting of Si and agarose after thermal annealing. (d) Stress-strain curves of agarose and PVdF films.

As a supplementary experiment to explore the potential applicability of agarose binder, we investigated interfacial adhesive behavior between agarose film and Si wafer, where the agarose film was directly deposited on the Si wafer through spin coating method. As a control sample, a PVdF film was chosen (fig. 2a and 2b). When the films were subjected to peel-off test using 3M scotch tape, the PVdF film was completely detached from the Si wafer. By comparison, the agarose film was still adhered to the Si wafer. Such stronger adhesive behavior of the agarose was further verified by analyzing characteristic peaks of Fourier transform infrared (FT-IR) spectra. As-synthesized Si particles showed typical vibration bands of silica materials (here, native silicon oxide) such as the Si-O-Si asymmetric stretching band at 1176 cm^{-1} and Si-O symmetric stretching band at 885 cm^{-1}.[30,32] On the other hand, the agarose film showed a broad peak at ~3420 cm^{-1} corresponding to hydroxyl group (O-H stretching vibrations) and a peak at 1070 cm^{-1} (related to C-O-C asymmetric vibrations) (fig. 2c, bottom). When the agarose/Si composite films were thermally annealed at 150 ^{o}C for 2 h, the peak intensity at ~3420 cm^{-1} (assigned to hydroxyl group) was significantly weakened, indicating the strong interaction between agarose and Si surface. Such strong interfacial interaction is anticipated to be favorable for enhancing the Si anode integrity and thus mitigating disruption of electrical network. Furthermore, agarose film, driven by inter- and intra-hydrogen bonding of its functional groups, has higher stiffness than PVdF film (fig. 2d), which is also expected to exert beneficial influence on cycling performance of Si anodes.

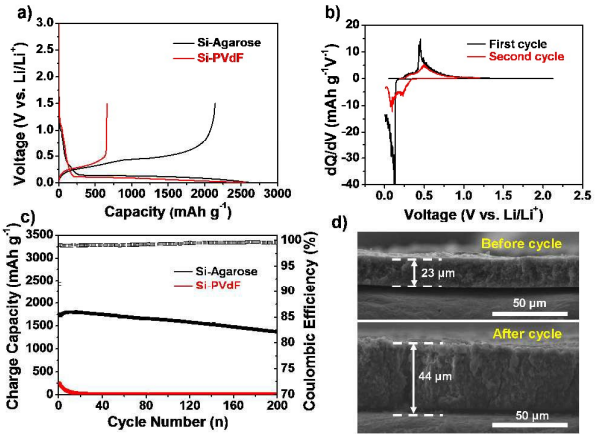

Fig. 3 Electrochemical performances of nanostructured Si anodes using agarose and PVdF binder. (a) First cycle voltage profiles in range of 0.005-1.5 V at a rate of 0.05C. (b) dQ/dV plots of first and second cycles. (c) Cycling performances of Si electrodes in range of 0.01-1.2V at a rate of 0.2C. (d) Cross-sectional SEM images of Si electrodes before (top) and after 200 cycles (bottom).

The electrochemical performances of Si anodes comprising the nanostructured Si powders and agarose binder were evaluated using a coin-type half cell under a voltage range of 0.005-1.5 V (versus Li/Li^{+}). Figure 3a shows the first cycle voltage profiles of Si electrodes at a discharge/charge current density of 0.05C/0.05C. In comparison to the Si anode with the PVdF binder, the Si anode incorporating the agarose binder showed considerable improvement in charge capacity/initial coulombic efficiency (2172 mAh g^{-1}/82.6% (agarose) vs. 658 mAh g^{-1}/25.8% (PVdF)). The stronger adhesive strength of agarose (shown in fig. 2) is expected to suppress the volume change-induced structural disruption (e.g., disintegration of electronic network and detachment of Si powders from copper current collectors) of the Si anodes, thus contributing to such better electrochemical performance.

The dQ/dV plots of the Si anodes are shown in fig. 3b. A sharp peak was observed at around 0.07 V with an onset potential of ~0.12 V during a first lithiation process, which was attributed to the phase transition of crystalline Si to amorphous lithium silicide (Li_xSi).[43] During the second lithiation, two different peaks respectively appeared at 0.24 V and 0.09 V, which may indicate the phase transitions between amorphous Li_xSi (i.e., transition from LiSi phase to Li_7Si_3 phase and subsequent transition to $Li_{15}Si_4$ phase.[44] Meanwhile, the dQ/dV plots of the first and second delithiation showed the characteristic peaks at ~0.28 V and ~0.45 V, exhibiting the occurrence of the de-alloying reaction $Li_{15}Si_4$ to Li_7Si_3 and Li_7Si_3 to LiSi.[43,44]

The synergistic coupling of nanostructured Si and agarose binder was highlighted in the cycling performance. The Si electrode incorporating the agarose binder presented the charge capacity of

1380 mAh g^{-1} (capacity retention = 71%) after 200 cycles under 0.2C/0.2C (fig. 3c). In contrast, the Si anode with PVdF binder showed a sharp capacity decay mainly due to the poor adhesion between PVdF and Si (shown in fig. 2). Notably, the strong adhesive force of agarose binder effectively suppressed the volume expansion (~95%) of Si anodes after 200 cycles (fig. 3d). In contrast, the PVdF binder-incorporated Si anode showed a significant expansion (170%) after 200 cycles (ESI, Fig. S1). Top surface of Si electrode with PVdF binder showed thicker SEI layers on the Si surfaces than that with agarose binder (ESI, Fig. S2). In addition to the improvement of cycling performance, the Si anode containing the agarose binder showed the superior rate capabilities, reaching a high capacity of 1000 mAh g^{-1} at current density of 3 C (ESI, Fig. S3).

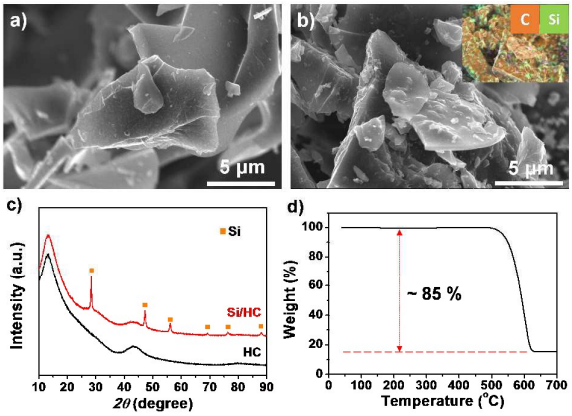

Fig. 4 SEM images of (a) as-synthesized HC and (b) Si/HC composite (inset: EDS mapping image). (c) XRD patterns of HC and Si/HC. (d) TGA analysis of Si/HC composite.

Synthesis and electrochemical characterization of Si/(agarose-derived) hard carbon composites

The hard carbon (HC) powders were prepared by a simple carbonization process (at 900 °C for 2 h in argon atmosphere) of agarose hydrogel. Figure 4a shows that the flake-shaped HC particles with lateral dimension of 1-10 μm were synthesized. Meanwhile, to obtain Si/HC composite materials, the nanostructured Si particles (shown in fig. 1) were mixed with agarose powder in dimethyl sulfoxide (DMSO). After removing DMSO through evaporation, the Si/agarose mixture was subjected to carbonization at 900 °C. The synthesized Si/HC powders showed similar morphologies and dimensions as those of the pure HC particles (fig. 4b). The energy-dispersive X-ray spectroscopy (EDS) mapping demonstrates that the Si particles are uniformly dispersed in the HC matrix (inset of fig. 4b). The XRD patterns of Si/HC powders showed the characteristic peaks corresponding to crystalline Si and amorphous hard carbon (fig. 4c). From the thermogravimetric analysis (TGA) profiles, the Si content in the Si/HC powders was estimated to be 15 wt% (fig. 4d). Future works will be devoted to controlling the composition ratio of Si/HC powders.

The anodes incorporating the HC powders (or Si/HC composite ones) and agarose binder were fabricated and their electrochemical performances of the HC and Si/HC composite anodes were investigated using coin-type half cells. Figure 5a shows that, under voltage range of 0.005 - 2.0 V and discharge/charge current density of 0.05C/0.05C, the discharge/charge capacities of the HC anode and Si/HC composite one at 1st cycle were 543/389 mAh g^{-1} (coulombic efficiency = 71.6%) and 654/513 mAh g^{-1} (coulombic efficiency = 78.4%), respectively. Subsequently, the anodes were further cycled under voltage range of 0.01 – 1.5 V and discharge/charge current density of 0.2C/0.2C. The HC anode showed good capacity retention with cycling, however, its reversible capacity was still unsatisfactory (300 mAh g^{-1} after 100 cycles). By comparison, the Si/HC composite anode provided the substantial increase in the reversible capacity (~490 mAh g^{-1}) and also excellent cycling performance (capacity retention after 100 cycles ~100%) (fig. 5b).

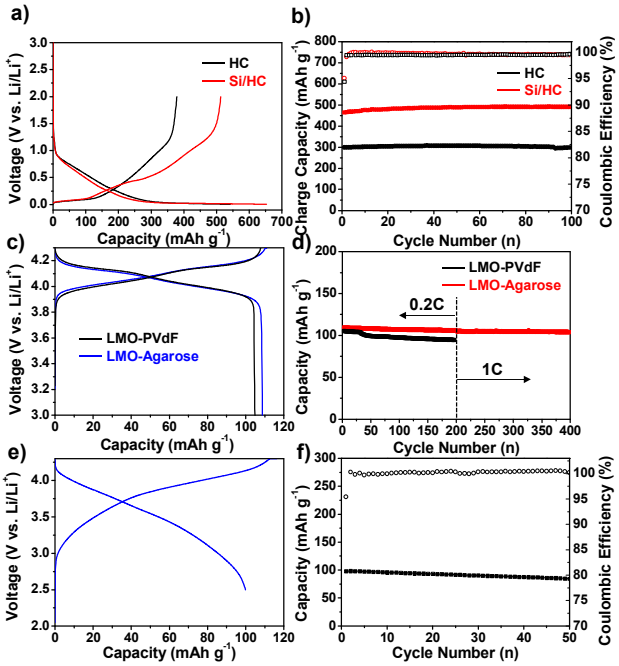

Fig. 5 (a) First cycle voltage profiles of HC and Si/HC anodes at a rate of 0.05C. (b) Cycle retentions of HC and Si/HC anodes at a discharge/charge rate of 0.2C/0.2C. (c) First charge and discharge voltage profiles of LMO cathodes at a rate of 0.05C. (d) Cycling performances of LMO-agarose and LMO-PVdF electrodes at charge/discharge rates of 0.2C/0.2C (1-200 cycles) and 1C/1C (201-400 cycles). (e) First cycle charge/discharge profile of full-cell (Si/HC anode and LMO cathode) at a rate of 0.05C. (f) Cycling performance of the full cell at a charge/discharge rate of 0.2C/0.2C.

Application of agarose as an alternative binder for LMO cathode and electrochemical performance of a full cell composed of Si/C anode and LMO cathode

In addition to the agarose application to the anode components mentioned above, agarose was also used as an alternative polymeric binder for LMO cathode. Under voltage range of 3.0 – 4.3 V and charge/discharge current density of 0.05C/0.05C, the charge and discharge capacities of the LMO cathode at 1st cycle were observed to be 105 mAh g^{-1} and 101 mAh g^{-1} with a high initial coulombic efficiency of 96.2% (Fig. 5c). The effect of binders on the

cycling performance of the LMO cathodes were investigated at charge/discharge current density of 0.2C/0.2C (1^{st} – 200^{th} cycle). Figure 5e shows that the agarose binder provided the exceptional capacity retention (~100%), as compared to the PVdF binder (~90%). Moreover, the LMO cathode incorporating the agarose binder maintained the good cycling performance even at faster charge/discharge current density of 1.0C/1.0C.

In order to elucidate the superior cycling performance of agarose binder-incorporated LMO electrode, Mn^{2+} chelation by the agarose and PVdF was investigated. For this experiment, the agarose and PVdF films were prepared through traditional solvent casting method and then immersed in manganese perchlorate solution. The absolute amount of Mn^{2+} ions captured by the films was quantitatively analysed by inductively coupled plasma (ICP) mass spectrometry (ESI, Fig. S4a). The agarose film effectively chelated the Mn^{2+} ions (921 ppm) compared to the PVdF film (2 ppm). Such excellent Mn^{2+}-chelating ability of the agarose film was further verified by the X-ray photoelectron spectroscopy (XPS) spectra (ESI, Fig. S4b). The agarose film showed the characteristic XPS peaks at 655 eV (assigned to Mn $2P_{1/2}$) and 643 eV (Mn $2P_{3/2}$),[45] demonstrating the existence of Mn^{2+} ions captured by the agarose. By comparison, the PVdF film did not show any traceable peaks in the Mn 2P region. These ICP and XPS results demonstrate that the agarose binder, which can effectively chelate Mn^{2+} ions, plays a viable role in achieving the excellent cycling performance over the conventional PVdF binder.

Based on the understanding of such unusual chelating effects of agarose, the cycled LMO cathodes and Li metal anodes (after 200 cycles) were characterized, with a focus on formation of by-products such as MnF_2. The MnF_2 by-products are known to be generated by side reactions between dissolved Mn^{2+} ions and hydrofluoric acid (originating from decomposition of $LiPF_6$-containg electrolytes).[46] The comparison in surface morphology of the cycled cathodes (ESI, Fig. S5) shows that the agarose-incorporated LMO cathode is relatively clean and less contaminated by unwanted by-products, in comparison to the control LMO cathode having the PVdF binder. This morphological difference between the LMO cathodes was confirmed by the ICP-MS results. The smaller amount of F element (indicative of MnF_2 formation on the cathode surface) was detected at the agarose-LMO cathode, demonstrating the superior Mn^{2+}-chelating ability of agarose binder. In addition, as another evidence to verify this advantageous effect of agarose binder, surfaces of the Li metal anodes (after 200 cycles) were analysed using ICP-MS. The Li metal anode which was assembled with the agarose-LMO cathode showed the smaller amount of Mn (8.1 ppm) than that (Mn = 35.5 ppm) combined with the control LMO cathode. The aforementioned results underscore the exceptional contribution of agarose binder to Mn^{2+} chelation.

Finally, a full cell composed of Si/HC anode (with agarose binder) and LMO cathode (with agarose binder) was fabricated and its electrochemical performance was characterized. Figure 5e shows first charge/discharge profile of the full cell, which were measured under voltage range of 2.5 – 4.3 V and charge/discharge current density of 0.05C/0.05C, were 116 mAh g^{-1} and 100 mAh g^{-1}, respectively. Subsequently, the cell was cycled at charge/discharge current density of 0.2C/0.2C and provided the stable cyclability (capacity retention after 50 cycles ~87%).

Conclusions

We demonstrated the exceptional multifunctionalites of eco-friendly and naturally abundant agarose for potential use as an alternative binder for Si anode/$LiMn_2O_4$ cathode and a carbon source for hard carbon. The agarose containing many functional groups provided a strong adhesion between active materials and current collectors, thereby alleviating the large volume change of Si-based anode materials during repeated charge/discharge cycling. The resulting agarose binder-incorporated Si anodes showed the significantly enhanced electrochemical properties (the high specific capacity of 1380 mAh g^{-1} (corresponding to capacity retention of 71% after 200 cycles). Also, the $LiMn_2O_4$ cathode assembled with the agarose binder exhibited high initial coulombic efficiency of 96.2% and stable cycling performance with capacity retention of nearly 100% after 400 cycles. Moreover, the agarose binder-incorporated full cell (consisting of Si/HC anode and $LiMn_2O_4$ cathode) exhibited highly stable cycling property (capacity retention after 50 cycles = 87%). We believe that the agarose featuring the aforementioned multifunctionality (as alternative binders and carbon sources) is highly effective and also versatile as an alternative green battery material, which thus can be easily extended to next-generation high-capacity anode materials (suffering from large volume change) and also high-capacity/high-voltage cathode ones (experiencing metal ion dissolution).

Experimental

Synthesis of nanostructured Si particles

10.0 g of Al-Si alloy powder (325 mesh, 99%, Al:Si = 88:12 wt.%, Alfa Aesar) was immersed in 400 mL of 3 M hydrochloric acid (HCl) solution (Samchun chemical, Korea) for 1 h with stirring. The chemically etched powders were filtered, rinsed with deionized (DI) water several times and then dried at 70 °C for 12 h. Finally, we obtained the nanostructured Si powders with a yield of 11%.

Synthesis of hard carbon

2.0 g of agarose (from Sigma-Aldrich) was dissolved into 60 mL of DI water with stirring at 95 °C for 1 h. The solution became transparent and then it was transferred to a petri dish for gelation at room temperature for 1 h. The resultant product was dried at 70 °C for 12 h in a convection oven. Subsequently, carbonization process of the agarose film was performed in a quartz tube furnace with ramping rate of 5 °C min^{-1}. The dried agarose film was heated to 500 °C for 1 h under an argon atmosphere for stabilization and further increased to 900 °C for 2 h to make hard carbon (HC) powders.

Synthesis of Si/HC composite

0.07 g of Si was dispersed in 25 mL of dimethyl sulfoxide (DMSO) with stirring and then ultra-sonicated at room temperature for 1 h. Subsequently, 2.16 g of agarose was added into the

aforementioned solution with stirring at 70 °C for 1 day. Then it was transferred to a glass petri dish for evaporation of solvent at 150 °C for 1 day. In a final step, carbonization process was performed in the similar manner with that of hard carbon.

Physicochemical characterization

Scanning electron microscopy (SEM, S-4800, Hitachi) was used to characterize morphologies of Al-Si, nanostructured Si, and Si/HC samples. To investigate the microstructures of samples, X-ray diffractometer (XRD, D8 Advance, Bruker, Cu Kα radiation) was used in the range of 10-90° at a scan rate of 1.4° s^{-1}. The nitrogen adsorption-desorption isotherms were measured with a VELSORP-mini II (BEL Japan, Inc.) at 77 K in the relative pressure range of P/P_0 from 0.05 to 0.3 to examine the BET surface areas and pore size distribution. Total reflectance–Fourier transform infrared (FT-IR) spectra of electrodes were recorded in a reflectance mode using a Varian 670-IR spectrometer with a spectral resolution of 4 cm^{-1} under a nitrogen atmosphere. The stress-strain curves of agarose and PVdF films were measured using a universal testing machine (AGS-100NX, SHIMADZU). Thermogravimetric analyzer (TGA, TA Instruments, USA) was used to measure the amount of carbon in the Si/carbon composite in the temperature range of 40-700 °C with a ramping rate of 5 °C min^{-1} in air.

Electrochemical test

The Si anode was prepared by mixing 70 wt% active material, 15 wt% of super P, and 15 wt% of binder with a mixer (Thinky mixer, ARE310) at 2200 rpm for 15 min to homogenize slurry mixture. The HC and Si/HC composite anodes were composed of active materials, super P, and agarose binder at a weight ratio of 80:10:10. The cathode ($LiMn_2O_4$) was made of 85 wt% of active material ($LiMn_2O_4$), 10 wt% super P, and 5 wt % of binder. After the slurries were casted on copper or aluminium foil, the electrodes were dried at 150 °C for 12 h in a vacuum oven to evaporate DMSO solvent. The mass loading levels of Si, Si/HC, HC, and $LiMn_2O_4$ in electrodes were 1.0, 1.9, 2.2, and 2.3 mg cm^{-2}, respectively. The coin-type half cell (2016R) and full-cell (2032R) were assembled in an argon-filled glove box. The Li metal foil was used as counter electrode and micro porous polyethylene film (Celgard 2400) was used as a separator. The electrolyte consisted of a solution of 1.3M $LiPF_6$ in a mixture of ethylene carbonate (EC)/diethyl carbonate (DEC) (3:7, v/v) with 10% fluorinated ethylene carbonate (FEC) additive in Si, Si/HC, and HC half-cells. In $LiMn_2O_4$ half-cell, the electrolytes consisted of 1M $LiPF_6$ in a mixture of EC/dimethyl carbonate (DMC) (3:7, v/v). The coin-type full-cell consisted of Si/HC anode, $LiMn_2O_4$ cathode, separator, and electrolyte. The electrolytes were composed of 1.3M $LiPF_6$ in a mixture of EC/ethylmethyl carbonate (EMC)/ DEC (3:4:3, v/v/v) with 5 wt% FEC additive and 0.5% tris(trimethylsilyl)phosphate (TMSP) additive. Galvanostatic charge and discharge cycling (WonATech WBCS 3000 battery measurement system) was performed at 25 °C.

Acknowledgements

This work was supported by Basic Science Research Program through the National Research Foundation of Korea funded by the Ministry of Science, ICT and future Planning (NRF-2015-01003143 and 2015R1A2A1A01003474).

Notes and References

1. J.-M. Tarascon and M. Armand, *Nature* 2001**, 414**, 359-367.
2. F. Cheng, J. Liang, Z. Tao and J. Chen, *Adv. Mater.* 2011**, 23**, 1695-1715.
3. B. Dunn, H. Kamath and J.-M. Tarascon, *Science* 2011**, 334**, 928-935.
4. V. Etacheri, R. Marom, R. Elazari, G. Salitra and D. Aurbach, *Energy Environ. Sci.* 2011**, 4**, 3243-3262.
5. M. R. Palacin, *Chem. Soc. Rev.* 2009**, 38**, 2565-2575.
6. M.-K. Song, S. Park, F. M. Alamgir, J. Cho and M. Liu, *Mater. Sci. Eng. R* 2011**, 72**, 203-252.
7. C. M. Park, J. H. Kim, H. Kim and H. J. Sohn, *Chem. Soc. Rev.* 2010**, 39**, 3115-3141.
8. U. Kasavajjula, C. Wang and A. J. Appleby, *J. Power Sources* 2007**, 163**, 1003-1039.
9. A. Magasinski, P. Dixon, B. Hertzberg, A. Kvit, J. Ayala and G. Yushin, *Nature Mater.* 2010**, 9**, 353-358.
10. C. K. Chan, H. Peng, G. Liu, K. McIlwrath, X. F. Zhang, R. A. Huggins and Y. Cui, *Nat. Nanotechnol.* 2007**, 3**, 31-35.
11. S. P. V. Nadimpalli, V. A. Sethuraman, S. Dalavi, B. Lucht, M. J. Chon, V. B. Shenoy and P. R. Guduru, *J. Power Sources* 2012**, 215**, 145-151.
12. S. Dalavi, P. Guduru and B. L. Lucht, *J. Electrochem. Soc.* 2012**, 159**, A642-A646.
13. V. Etacheri, O. Haik, Y. Goffer, G. A. Roberts, I. C. Stefan, R. Fasching and D. Aurbach, *Langmuir* 2012**, 28**, 965-976.
14. R. Huang, X. Fan, W. Shen and J. Zhu, *Appl. Phys. Lett.* 2009**, 95**, 133119.
15. S. Choi, J. C. Lee, O. Park, M.-J. Chun, N.-S. Choi and S. Park, *J. Mater. Chem. A* 2013**, 1**, 10617-10621.
16. C.-H. Yim, F. M. Courtel and Y. Abu-Lebdeh, *J. Mater. Chem. A* 2013**, 1**, 8234-8243.
17. D. Shao, D. Tang, Y. Mai and L. Zhang, *J. Mater. Chem. A* 2013**, 1**, 15068-15075.
18. S. L. Yuezeng Su, Dongqing Wu, Fan Zhang, Haiwei Liang, Pengfei Gao, Chong Cheng, and Xinliang Feng, *ACS Nano* 2012, **6**, 8349-8356.
19. S. Li, D. Wu, C. Cheng, J. Wang, F. Zhang, Y. Su and X. Feng, *Angew. Chem. Int. Ed.* 2013, **52**, 12105-12109.
20. L. Hu, H. Wu, S. S. Hong, L. Cui, J. R. McDonough, S. Bohy and Y. Cui, *Chem. Commun.* 2011**, 47**, 367-369.
21. C. K. Chan, R. Ruffo, S. S. Hong, R. A. Huggins and Y. Cui, *J. Power Sources* 2009**, 189**, 34-39.
22. M.-H. Park, M. G. Kim, J. Joo, K. Kim, J. Kim, S. Ahn, Y. Cui and J. Cho, *Nano Lett.* 2009**, 9**, 3844-3847.
23. A. Esmanski and G. A. Ozin, *Adv. Funct. Mater.* 2009**, 19**, 1999-2010.
24. Y. Yao, M. T. McDowell, I. Ryu, H. Wu, N. Liu, L. Hu, W. D. Nix and Y. Cui, *Nano Lett.* 2011**, 11**, 2949-2954.

25. N. Liu, H. Wu, M. T. McDowell, Y. Yao, C. Wang and Y. Cui, *Nano Lett.* 2012, **12**, 3315-3321.
26. W.-R. Liu, M.-H. Yang, H.-C. Wu, S. M. Chiao and N.-L. Wu, *Electrochem. Solid-State Lett.* 2005**, 8**, A100-A103.
27. L. Xie, L. Zhao, J.-L. Wan, Z.-Q. Shao, F.-J. Wang and S.-Y. Lv, *J. Electrochem. Soc.* 2012**, 159**, A499-A505.
28. N.-S. Choi, K. H. Yew, W.-U. Choi and S.-S. Kim, *J. Power Sources* 2008**, 177**, 590-594.
29. A. Magasinski, B. Zdyrko, I. Kovalenko, B. Hertzberg, R. Burtovyy, C. F. Huebner, T. F. Fuller, I. Luzinov and G. Yushin, *ACS Appl. Mater. Interfaces* 2010**,** 2, 3004-3010.
30. I. Kovalenko, B. Zdyrko, A. Magasinski, B. Hertzberg, Z. Milicev, and R. Burtovyy, I. Luzinov and G. Yushin, *Science* 2011**, 334**, 75-79.
31. Z.-J. Han, N. Yabuuchi, K. Shimomura, M. Murase, H. Yui and S. Komaba, *Energy Environ. Sci.* 2012**, 5**, 9014-9020.
32. B. Koo, H. Kim, Y. Cho, K. T. Lee, N. S. Choi and J. Cho, *Angew. Chem. Int. Ed.* 2012**, 51**, 8762-8767.
33. C. Kim, J. Y. Jang, N.-S. Choi and S. Park, *RSC Adv.* 2014**, 4**, 3070-3074.
34. Y. K. Jeong, T. W. Kwon, I. Lee, T. S. Kim, A. Coskun and J. W. Choi, *Nano Lett.* 2014**, 14**, 864-870.
35. S.S. Zhang and T. R. Jow, *J. Power Sources* 2002**, 109**, 422-426.
36. M.-H. Ryou, S. Hong, M. Winter, H. Lee and J. W. Choi, *J. Mater. Chem. A* 2013**, 1**, 15224-15229.
37. K.-F. Chiu, S. H. Su, H.-J. Leu and Y. S. Chen, *Electrochim. Acta* 2014**, 117**, 134-138.
38. S. Arnott, A. Fulmer, W. E. Scott, I. C. M. Dea, R. Moorhouse and D. A. Rees, *J. Mol. Biol.* 1974**, 90**, 269-272.
39. M. Lahaye and C. Rochas, *Hydrobiologia* 1991**, 221**, 137-148.
40. J.-M. Kim, C. Kim, S. Yoo, J.-H. Kim, J.-H. Kim, J.-M. Lim, S. Park and S.-Y. Lee, *J. Mater. Chem. A* 2015**, 3**, 10687-10692.
41. W. Zhou, T. Jiang, H. Zhou, Y. Wang, J. Fang and M. S. Whittingham, *MRS Commun.* 2013**, 3**, 119-121.
42. G. Hwang, H. Park, T. Bok, S. Choi, S. Lee, I. Hwang, N.-S. Choi, K. Seo and S. Park, *Chem. Commun.* 2015**, 51**, 4429-4432.
43. M. N. Obrovac and L. J. Krause, *J. Electrochm. Soc.* 2007**, 154**, A103-A108.
44. M. K. Datta and P. N. Kumta, *J. Power Sources* 2009**, 194**, 1043-1052.
45. M.-H. Ryou, S. Hong, M. Winter, H. Lee and J. W. Choi, *J. Mater. Chem. A* 2013, **1**, 15224-15229.
46. C. Zhang, J. Lu, K. A. Jeremy, T. Wu, A. N. Jansen, Y. K. Sun, X. Qiu, K. Amine, *Nature Commun.* 2013, **4**, 2437.

Graphical abstract :

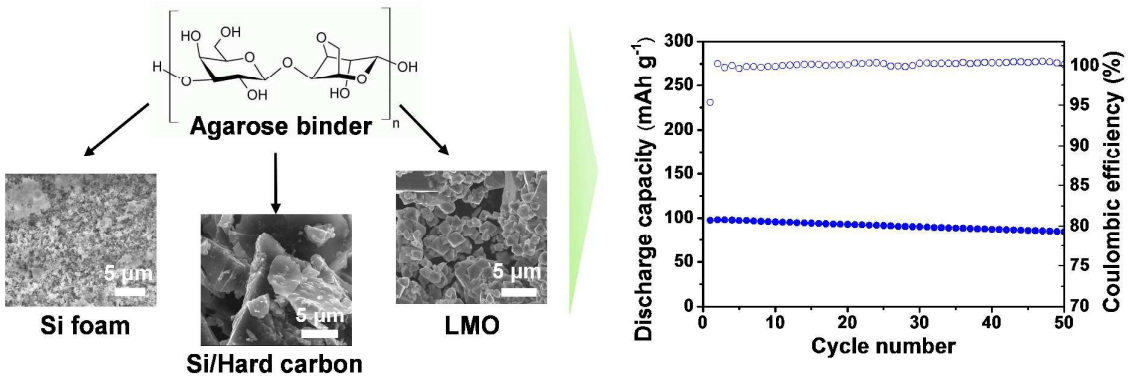

Multifunctional agarose act as effective binder for Si anode and $LiMn_2O_4$ cathode and also serve good carbon source to make hard carbon. Also, agarose-assisted full-cell consisting of Si/C anode and $LiMn_2O_4$ cathode shows a stable cycling performance.